Observation of a Total Eclipse of the Moon at 89 and 183 GHz

Martin Burgdorf[1]*, **Niutao Liu[2]**, **Stefan A. Buehler[1]**, **and Ya-Qiu Jin[2]**

[1]Universität Hamburg, Meteorologisches Institut, Bundesstraße 55, 20146 Hamburg, martin.burgdorf@uni-hamburg.de

[2]Key Laboratory of Information Science of Electromagnetic Waves, Ministry of Education, Fudan University, Shanghai 200433, China, ntliu@fudan.edu.cn

Key Points:

- The Moon appeared in the deep space view of AMSU-B on NOAA-15 during the lunar eclipse in Oct 2004.
- Its disk-integrated brightness temperature was measured at 89 and 183 GHz in intervals of 100 min.
- The radiance is in good agreement with predictions from a new model.

---

*Deutsche Forschungsgemeinschaft

Corresponding author: Martin Burgdorf, `martin.burgdorf@uni-hamburg.de`

Abstract

The total lunar eclipse from October 28, 2004, was observed by AMSU-B (Advanced Microwave Sounding Unit - B) on NOAA-15 during a couple of minutes of each orbit around the Earth. From this unique vantage point in space it could provide disk-integrated, effective lunar temperatures at lower frequencies than employed in most previous observations of eclipses, in intervals of 100 min. The relative changes in brightness temperature were 6.4±2.1 % at 89 GHz and 16.6±2.1 % at 183 GHz. This trend of stronger temperature drop at higher frequency was expected on the basis of a new radiative transfer model simulating the global brightness temperatures. Our measurements disprove two results published in the past, but they confirm the claim made before that the changes are similar at the center and for the whole disc. In terms of precision they are comparable to those carried out in the past with radio telescopes on ground.

Plain Language Summary

The observation of an eclipse of the Moon at millimeter wavelengths makes it possible to investigate the electrical and thermal properties of the lunar crust to a depth of 10 cm without being influenced by deeper layers. Such measurements are usually carried out with radio telescopes on Earth. When microwave instruments on weather satellites use observations of deep space for their calibration, however, the whole lunar disk appears sometimes in their field of view as well. We identified such an event that coincided with a total lunar eclipse. From this unique vantage point in orbit around the Earth we could measure, once per orbit, the lunar radiance at 183 GHz - a frequency, where the atmosphere is not transparent. We found a maximum temperature drop during the eclipse of 47.9 K and overall agreement of the evolution of the global flux with the predictions from theoretical studies. Our measurements are consistent with results reported in the past, except for two, which we consider erroneous. The temperature changes are similar everywhere on the lunar disc. The good agreement between the observations from a weather satellite and theoretical predictions demonstrates that the Moon is very useful for checking the reliability of climate data records from Earth observation.

1 Introduction

The Advanced Microwave Sounding Units (AMSU-A and -B) were the first microwave sounders that could detect the Moon with good signal-to-noise ratio during routine operations. Such observations happen serendipitously, when the Moon enters the deep space view (DSV), i. e. the pointing direction used for measuring the signal from the Cosmic Microwave Background for the purpose of flux calibration. The opportunity for this to happen arises at most twice per month, and lunar flux is then usually received in several consecutive orbits. AMSU-B on NOAA-15 observed the Moon this way during the total eclipse from October 28, 2004, in its channels at 89, 150, and 183 GHz. This coincidence - the only one of this kind we could find - provided unique data, because the atmosphere is not transparent at 183 GHz, and therefore observations at this frequency are not possible with radio telescopes on ground.

At frequencies higher than this water vapor line, however, it is possible to observe radio eclipses of the Moon from the ground, and this was done several times in the past. There is disagreement among the results reported from these campaigns. The latest stab at measuring such an event at millimeter wavelengths was carried out by Pardo et al. (2005), who used the Caltech Submillimeter Observatory on Mauna Kea, Hawaii, to observe the center of the lunar disk between 165 and 365 GHz during the eclipse on July 16, 2000. Unfortunately they did not get any useful data after 13:02 UT, the beginning of totality. Their result of a temperature drop during the eclipse at a frequency of 240 GHz being 18% is therefore only a lower limit and could not finally settle the question which one of the other measurements was closest to the truth.

Most of these results were supported by model calculations so that a decision on who got it right implies a better understanding of the upper 10 cm of the lunar regolith. The obstacles encountered with previous measurements were in part of an instrumental nature, because the equipment was not up to today's standards, and in part caused by variations of the atmospheric conditions. Satellite observations do not have these problems, and therefore the lunar eclipse mentioned at the beginning of this section seemed like a good opportunity to get the story straight. Although AMSU-A and -B can only make disk-integrated measurements of the Moon, they are not necessarily at a disadvantage when compared to astronomical observatories, because the temperature drops are similar over most of the lunar disk. As AMSU-B has a smaller beam than AMSU-A, it provides a better signal-to-noise ratio when observing the Moon, and therefore we limited our investigation to this instrument. We compared our measurements with the predictions of a radiative transfer model of the lunar regolith. For this purpose the heat conductive equations were solved, and we calculated the global lunar temperatures and brightness temperatures with the thermal-physical parameters derived from Diviner infrared data and loss tangents from Chang'e 2 microwave data.

2 Materials and Methods

The level 1b data from AMSU-B on NOAA-15 are publicly available from NOAA's Comprehensive Large Array-data Stewardship System (CLASS). The digital counts obtained from the DSV, when the Moon moved through the FoV (Field of View), are calibrated by interpolating between the counts obtained from the internal calibration source and those from the DSV without Moon in the FoV. Taking the beam size and the apparent diameter of the lunar disk into account as well, it is then possible to calculate the flux density and with Planck's law the brightness temperature (Yang & Burgdorf, 2020). We applied the AMSU-B RFI (radio frequency interference) corrections from Table M9-11 in `http://rain.atmos.colostate.edu/XCAL/docs/amsub/NOAA_KLM_Users_Guide.pdf` to the measured digital counts; this procedure resulted in changes to the brightness temperatures in the order of one percent. As all observations of the lunar eclipse were carried out with the same mean power of all transmitters, the RFI affected all of them in the same way and left the measured changes in radiance unaltered.

2.1 Observations

The exact timing of the eclipse and its observations with NOAA-15 are given in Table 1. AMSU-B receives radiation from the Moon, when at least one of its four deep space views points close to its position. During one orbit, the pointing directions of the four deep space views describe four concentric circles in the sky around the orbital axis of the satellite - for an illustration see Figure 1 in Bonsignori (2017). On 10/27, 2004, the Moon approached these circles and its radiation began to reach the receivers for a few minutes of every orbit. The Moon appeared first in DSV 1 and advanced by about half a degree during each orbit of NOAA-15. This means that it was close to the center of the FoV at 0:50, 4:15, and 7:39 of 10/28, 2004, and in between two DSVs at the other times in Table 1. In the latter configuration a correction had to be applied to the digital counts, because they were much lower than when the Moon was in the center of the FoV. This correction increased the uncertainty of the calculated brightness temperature.

2.2 Calculation of Lunar Flux Density

As the shape of the beam pattern resembles a Gaussian (`http://www-cdn.eumetsat.int/files/2020-05/pdf_mhs_char_data_des.pdf`) with a full width at half maximum (FWHM) of 1.1°, the signal produced by the Moon is almost the same for all positions closer than 0.1° to the center of the DSV. This was

Table 1. Time of the Total Eclipse of the Moon on October 28, 2004, and relevant observations with AMSU-B on NOAA-15. The shaft position of maximum signal indicates the position of the Moon in the scan direction; it can be compared to the pointing direction of the deep space views, which is 71 for DSV 1, 196 for DSV 2, 338 for DSV 3, and 485 for DSV 4. S-T-O is the Sun-Moon-NOAA-15 angle, it is negative for waxing and positive for waning Moon. The times have been obtained from `https://www.timeanddate.com/eclipse/lunar/2004-october-28`.

Event	Time (UTC)	Shaft Position	S-T-O
Moon in DSV of AMSU-B	23:08 (10/27)	130	$-4.3°$
Penumbral Eclipse began	00:07		
Moon in DSV of AMSU-B	00:50	210	
Partial Eclipse began	01:15		
Full Eclipse began	02:24		
Moon in DSV of AMSU-B	02:32	280	
Full Eclipse ended	03:44		
Moon in DSV of AMSU-B	04:15	348	
Partial Eclipse ended	04:53		
Moon in DSV of AMSU-B	05:57	407	
Penumbral Eclipse ended	06:01		
Moon in DSV of AMSU-B	07:39	460	$1.5°$

the case in our observations at 00:50 and 04:15, where we could correct for the small displacement as described in Burgdorf et al. (2021). The signal decreases steeply, however, when the Moon moves about FWHM/2 away from this center position. Instead of a strong signal in one of the four DSVs one obtains in this case weaker signals in two neighbouring DSVs. In this case it gets difficult to calculate the flux received from the Moon, because the beam pattern deviates from a Gaussian at large distance from its center, and the deep space views 2 and 3 are not equidistant from their left and right neighbours. For these reasons we decided to search for other Moon intrusions that gave a similar ratio between the counts in different DSVs to those obtained during the lunar eclipse. The phase angle of the Moon changes by less than 1° during one orbit of NOAA-15, and the change in flux is smallest, when the observations are made close to full Moon, because its brightness temperature is then almost at its highest. Assuming therefore a constant lunar flux in all measurements, we can directly calculate the effect of the exact position of the Moon in between the different deep space views on the digital counts. With the knowledge of how these counts depend on shaft position at constant radiance, we could determine the change in radiance due to the cooling of the lunar regolith during the eclipse. The observations of the Moon used as reference for the eclipse happened on Sep 18, 2005, Oct 15 thru 18, 2005, Feb 12 and 13, 2006, and Sep 26, 2007.

3 Data

For the conversion from digital counts to lunar brightness temperature it is important to know the apparent diameter of the Moon, and we obtained this information from the HORIZONS system by the Jet Propulsion Laboratory (`https://ssd.jpl.nasa.gov/?horizons`). It requires knowledge of the Nadir Position of NOAA-15, which is included in its level 1b data, and its altitude, which is included in the level 1b data of each satellite as well. Burgdorf et al. (2021) had calculated a random uncertainty of 2 K for a single measurement of the lunar radiance with MHS (Microwave Humidity Sounder) and about double this value for AMSU-B. This applies to the measurements of the eclipse at 00:50 and 4:15. For the reasons explained in section 2 there are systematic effects present in the other measure-

ments that are caused by the position of the Moon in between DSVs. From the scatter of the correction factors derived from different reference observations of the Moon during non-eclipse we concluded that these systematic effects contribute to the overall uncertainty, albeit to a lesser degree than the pure random effects. Unfortunately the sounding and window channels of AMSU-B have different quasi-optical paths and slightly different beam widths, therefore one cannot use the same correction factors for all of them. In addition to the random scatter of observed brightness temperatures Burgdorf et al. (2021) had found a positive bias of 5.5% in the disk-integrated flux density of the Moon as measured with MHS when compared to the model by Liu and Jin (2021a), so we have divided the flux densities at 89 GHz from AMSU-B by 1.05. At 183 GHz we divided the measured values by 1.08 to bring them into accord with the model. This systematic discrepancy of 3% between the absolute flux levels at 89 and 183 GHz when compared to the model could be due to an error of just 1.5% in the beam size of the sounding channels as determined from the duration of many lunar intrusions in the DSV. It does not affect, however, the value of the temperature drop during the eclipse, $(\Delta T_L/T_L)_{max}$.

In order to provide flux densities with a computer model to compare the observations with, the near side of the Moon surface was divided into 900 sub-regions with a span of $6° \times 6°$ in longitude and latitude. For simulating the solar irradiance, the Sun is divided into 10×20 meshes. The visibility of each mesh of the Sun for any given mesh of the Moon is then calculated. The solar radiation from each mesh is added up to determine the solar heat flow at a certain place on the moon. The total solar irradiance (TSI) can be written as

$$TSI = \frac{\sigma T_S^4 R_S^2}{D^2} \tag{1}$$

Where D is the distance between the Sun and the Moon (Liu & Jin, 2021b). T_S is the temperature of the Sun, R_S is its radius, and σ is the Stefan-Boltzmann constant. The solar radiation is assumed to be isotropic. TSI is 1371 W/m^2, when the distance between the Sun and the Moon is one astronomical unit. The actual distance between these two objects, as it changed during the eclipse, was used in our calculations. During a lunar eclipse, the received solar irradiance by the mesh j on the Moon can be written as:

$$TSI_j = \frac{\sigma T_S^4 \sum_{i=1}^{200} S_i v_{ij}}{2\pi D^2} \tag{2}$$

Where S_i is the area of the mesh i of the Sun and v_{ij} is its visibility from mesh j of the Moon. For the contribution from a single mesh i of the Sun to the solar irradiance received by mesh j of the Moon we get

$$\frac{\sigma T_S^4 R_S^2}{D^2} \cdot \frac{(\lambda_{i2} - \lambda_{i1})(\sin \phi_{i1} - \sin \phi_{i2})}{2\pi} \cdot v_{ij} \tag{3}$$

Where λ_{i1} and λ_{i2} are the longitudes of the left and right boundaries of mesh i of the Sun, and ϕ_{i1} and ϕ_{i2} are the latitudes of the upper and lower boundaries of mesh i of the Sun. In the next step, the one-dimensional heat conductive equation is solved, providing the temperature profile for each mesh of the Moon. Finally, the disk-integrated brightness temperature can be simulated with the radiative transfer model.
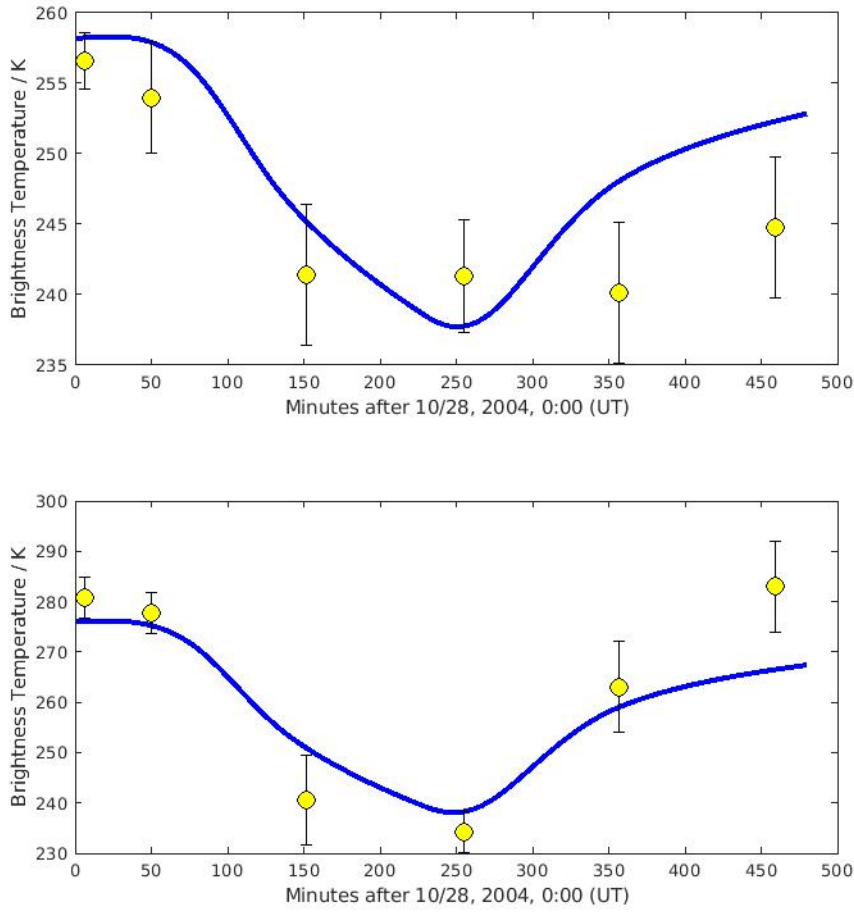
4 Results

In Figure 1 we show the changing brightness temperature of the Moon at 89 and 183 GHz during the eclipse and compare our measured values with the predictions of the model by Liu and Jin (2021a). At 150 GHz the signal-to-noise ratio was not good enough to produce meaningful results.

When the penumbral phase of an eclipse begins, the Sun becomes partially eclipsed by the Earth for more and more places on the Moon. The solar radiation is therefore weaker at these places, and consequently the local temperature of the uppermost layer begins to decrease rapidly. The local microwave brightness temperatures at 89 GHz and 183 GHz,

originating at greater depth, decrease as well, but slower because of the small heat conductivity. As a consequence, the temperature drop is small at these deep layers. The disk-averaged brightness temperature starts to decline about 15 min after the start of the penumbral phase.

When the partial phase of an eclipse begins, the Sun becomes fully eclipsed by the Earth for more and more places on the Moon, and the surface temperature continues dropping everywhere until the end of the full phase, when some places on the Moon start being illuminated by a narrow crescent of the Sun appearing behind the Earth. The temperatures of the uppermost layer and the radiance at 89 GHz and 183 GHz rise rapidly in these regions, followed by an increase in subsurface temperature at greater depths. As a consequence, the global microwave brightness temperature begins to increase about half an hour after the end of the full phase. In Figure 1, the microwave brightness temperature starts to increase on 10/28, 2004, at about 04:10 (UTC).

Figure 1. Disk-integrated brightness temperature of the Moon at 89 (top) and 183 GHz (bottom) during the total eclipse of October 28, 2004. Yellow circles: measurements with AMSU-B (Advanced Microwave Sounding Unit - B), blue line: prediction by a model (Liu & Jin, 2021a)

With the simulation, it can be found that $(\Delta T_L/T_L)_{max}$ increases with the surface heat conductivity. A larger heat conductivity will make the temperature decrease rapidly at depths of centimeters when the Sun is eclipsed by the Earth, although the temper-

Table 2. Lunar eclipse observations at microwaves. The third column gives the time span between start and end of full eclipse. The last column gives the maximum brightness temperature decrease. For Reber and Stacey (1969) the lower value at 88 GHz refers to Copernicus and the higher value to Mountain area, at 94 GHz the lower value refers to Mare Serenitatis and the higher value to Mountain area, and at 214 GHz the lower value refers to Copernicus and the higher value to Mare Serenitatis.

Reference	Date	Totality	Frequency	Beam Width	$(\Delta T_L/T_L)_{max}$
		min	GHz	min of angle	%
Kamenskaya et al. (1965)	12/30, 1963	79	75	20	12 ± 2
Reber and Stacey (1969)	12/30, 1963	79	94	2.8	$6.0 \pm 1.4 \; - \; 8.2 \pm 1.0$
Reber and Stacey (1969)	10/18, 1967	60	88	3.3	$5.8 \pm 0.4 \; - \; 8.0 \pm 0.9$
This study - model	**10/28, 2004**	**82**	**89**	**lunar disk**	8.0
This study - obs.	**10/28, 2004**	**82**	**89**	**73**	6.4 ± 2.1
Sinton (1956)	1/19, 1954	30	200	lunar disk	45
Baldock et al. (1965)	12/19, 1964	59	300	7	30 ± 5
Kamenskaya et al. (1965)	11/30, 1963	79	250	7	22.5 ± 2.5
Low and Davidson (1965)	12/19, 1964	59	250	3.9	9.8 ± 1.1
Reber and Stacey (1969)	10/18, 1967	60	214	1.78	$24.8 \pm 1.8 \; - \; 25.7 \pm 2.2$
Sandor and Clancy (1995)	11/29, 1993	47	226	0.5	25
Pardo et al. (2005)	7/16, 2000	106	240		≥ 18
This study - model	**10/28, 2004**	**82**	**183**	**lunar disk**	13.8
This study - obs.	**10/28, 2004**	**82**	**183**	**72**	16.6 ± 2.1

ature at deeper layers may still be higher than in the case of smaller heat conductivity. In addition, the loss tangent of the regolith will affect $(\Delta T_L/T_L)_{max}$ as well. An increase in loss tangent has a similar effect as an increase in frequency on the penetration depth.

5 Discussion

In Table 2 we place our results in context with earlier efforts. To our best knowledge we present here for the first time the microwave flux density during a total eclipse of the Moon obtained from Earth orbit. This special location allowed access to a wavelength in between those utilized by ground-based radio telescopes, viz. 183 GHz. Another unique feature of our observations is that the whole Moon was included in the FoV. We expect the effect of the eclipse to be similar all over the lunar disk - an assumption made already by Kamenskaya et al. (1965). This means that our results are suitable for comparison with those obtained with radio telescopes having much smaller beam size.

Sandor and Clancy (1995) observed the Moon with the radio telescope at Kitt Peak, Arizona, and they found its brightness temperature at 226 GHz to decrease a maximum of 25% during the eclipse of November 29, 1993. They pointed the telescope at the center of the lunar disk and at regions at 42° lunar latitude north and south, with a beam width of only 0.5'. Within the uncertainties of the measurement, the temperature drop was the same in all three cases, when normalized to the brightness temperature just before the eclipse. The same value had been found before by Reber and Stacey (1969) at 214 GHz with the lunar eclipse on October 18, 1967, when also pointing at three different positions on the lunar disk. These results differ considerably from earlier findings by Low and Davidson (1965), who reported a maximum temperature change of only 10% at 250 GHz for the eclipse on December 19, 1964. This small temperature drop is all the

229 more confusing, since the duration of totality on 12/19, 1964, was longer than on 11/29,
230 1993. Their result is at least four standard deviations off target.

231   From observations with different receivers a strong dependency of the lunar bright-
232 ness temperatures on frequency became apparent: Reber and Stacey (1969) detected tem-
233 perature changes between 6 and 8% at 88 GHz, i. e. less than a third of the value at 214 GHz.
234 Again the published results do not always agree: Kamenskaya et al. (1965) claimed a max-
235 imum relative drop in effective temperature of 12% at a slightly lower frequency for the
236 eclipse on December 30, 1963. This discrepancy is odd, given the fact that Reber and
237 Stacey (1969) observed Kamenskaya's eclipse as well.

238   Indeed our results for the ratio between the amplitude of the brightness temper-
239 ature drop during the eclipse $(\Delta T_L)_{max}$ and the brightness temperature at the start of
240 the eclipse T_L fit into the trend with frequency observed before. As the depth of the emit-
241 ting layer of the regolith of the Moon increases with wavelength, and deeper layers are
242 less affected by changes in temperature on the surface, we expect a slightly lower $(\Delta T_L/T_L)_{max}$
243 at 183 GHz than at the higher frequencies accessible from ground. This is exactly what
244 we find in Table 2: a temperature drop $(\Delta T_L/T_L)_{max}$ of 30% at 300 GHz, 25% at 226 GHz,
245 and our measured value of 17%, or 14% according to the model, at 183 GHz. (We note
246 that the slightly higher brightness temperature measured after the eclipse, see Figure 1,
247 might just have been something to do with the fact that the phase angle of the Moon
248 had changed by almost 6° compared to the beginning of this event, see Table 1). Extrap-
249 olating this trend to even smaller frequencies we expect of find $(\Delta T_L/T_L)_{max} \approx 8\%$ at
250 89 GHz, in agreement with all measurements, when the uncertainty is taken into account,
251 and our model. The only exception is the observation by Kamenskaya et al. (1965), with
252 a temperature drop almost double as high as the one observed by us.

253   Although our measurements were 100 min apart from each other, it is possible to
254 derive constraints on the moment in time, at which the Moon reached its lowest bright-
255 ness temperature - at least at 183 GHz, because at 89 GHz the signal-to-noise ratio is
256 not good enough. Both model and observation suggest that this point was reached half
257 an hour after full eclipse ended. This is quite compatible with the plots of lunar tem-
258 perature vs. time in King et al. (1966), which demonstrated a cooling trend that con-
259 tinued for 35 min after umbral exit at five different lunar areas. As AMSU-B could not
260 spatially resolve the lunar disk, certain regions reached the minimum value several min-
261 utes earlier and others later than in Figure 1, because the process of emerging from the
262 Earth's shadow takes more than one hour from end of full to end of partial eclipse.

263   The fact that the measured brightness temperature at 89 GHz does not change sig-
264 nificantly for four hours after the end of the full eclipse suggests a slower recovery from
265 the temperature drop caused by the eclipse than predicted by the model. Unfortunately
266 the signal-to-noise ratio in the measurements at low frequencies by Kamenskaya et al.
267 (1965) and Reber and Stacey (1969) was too poor to settle this question. We note, how-
268 ever, that also the amplitude of the annual variations of the brightness temperature of
269 the Moon at 89 GHz, which are caused by its changing distance to the Sun, was found
270 to be smaller in the measurements by Burgdorf et al. (2021) than predicted by Liu and
271 Jin (2019). In contrast, at 183 GHz the agreement between the two is almost perfect.
272 It will be interesting to see how well model and observations agree at frequencies below
273 89 GHz that are employed by other microwave sounders on polar orbits.

6 Conclusions

275   It is just a question of time, when a total eclipse of the Moon will be observed by
276 the generations of microwave sounders that follow AMSU-B, and these measurements
277 will be more precise than those with AMSU-B. For the time being, however, the model
278 by Liu & Jin of the disk-integrated radiance of the Moon reproduces the observations
279 of eclipses very well. This test of its performance is important, because an eclipse is the
280 only possibility to observe the Moon with a microwave sounder in an orbit around the
281 Earth, when it is not exposed to sunlight. The model reproduced also very well the mea-

sured dependence of the disk-integrated lunar brightness temperature T_L on phase angle, as observed with the Microwave Humidity Sounders on NOAA-18 and -19 (Burgdorf et al., 2021). As lunations last much longer than eclipses, the temperature changes with phase angle contain information about deeper layers of the regolith. Our study provides additional and unique proof for the usefulness of this model. Its accurate prediction of the disk-integrated flux density is not only relevant for checking the performance of weather satellites, but also for the calibration of astronomical radio telescopes with a large beam width, like the Cosmology Large Angular Scale Surveyor (Dahal et al., 2021).

Data Availability

The raw data from NOAA-15 are supplied by the NOAA Comprehensive Large Array-data Stewardship System at `https://www.class.noaa.gov/`. The thing to note here is that AMSU-B is not listed separately under the main product listing in CLASS. It is logically grouped under the TOVS data family found at the bottom of the drop down menu. One must select TOVS to get to the AMSU-B data product and then select the satellite on the "Search - TOVS" page. Access to the archive is free. There is no DOI for the raw data we used.

Acknowledgments

References

Baldock, R. V., Bastin, J. A., Clegg, P. E., Emery, R., Gaitskell, J. N., & Gear, A. E. (1965, April). Lunar Eclipse Observations at 1-MM Wavelength. *Astrophysical Journal*, *141*, 1289. doi: 10.1086/148257

Bonsignori, R. (2017). In-orbit verification of MHS spectral channels co-registration using the moon. In J. J. Butler, X. J. Xiong, & X. Gu (Eds.), *Earth observing systems xxii* (Vol. 10402, pp. 714 – 722). SPIE. Retrieved from `https://doi.org/10.1117/12.2273335` doi: 10.1117/12.2273335

Burgdorf, M. J., Buehler, S. A., & Prange, M. (2021, July). Calibration and Characterization of Satellite-Borne Microwave Sounders With the Moon. *Earth and Space Science*, *8*(7), e01725. doi: 10.1029/2021EA001725

Dahal, S., Appel, J. W., Datta, R., Brewer, M. K., Ali, A., Bennett, C. L., ... Xu, Z. (2021, July). Four-year Cosmology Large Angular Scale Surveyor (CLASS) Observations: On-sky Receiver Performance at 40, 90, 150, and 220 GHz Frequency Bands. *arXiv e-prints*, arXiv:2107.08022.

Kamenskaya, S. A., Kislyakov, A. G., Krotikov, V. D., Naumov, A. I., Nikonov, V. N., Porfir'ev, V. A., ... Sorokina, E. P. (1965, March). Observation of radio eclipses of the moon at millimeter wavelengths. *Radiophysics and Quantum Electronics*, *8*(2), 155-161. doi: 10.1007/BF01038602

King, H., Jacobs, E., & Stacey, J. (1966, January). A 2.8 arc-min beamwidth antenna: Lunar eclipse observations at 3.2 mm. *IEEE Transactions on Antennas and Propagation*, *14*(1), 82-91. doi: 10.1109/TAP.1966.1138630

Liu, N., & Jin, Y.-Q. (2019, November). Calibration of a multichannel millimeter wave radiometer of FY-4M based on the real-time brightness temperature along the lunar equator. *Science Bulletin*. doi: 10.1360/TB-2019-0200

Liu, N., & Jin, Y.-Q. (2021a, February). Average Brightness Temperature of Lunar

Surface for Calibration of Multichannel Millimeter-Wave Radiometer From 89 to 183 GHz and Data Validation. *IEEE Transactions on Geoscience and Remote Sensing*, *59*(2), 1345-1354. doi: 10.1109/TGRS.2020.3000230

Liu, N., & Jin, Y.-Q. (2021b, March). Calibration of the space-borne microwave humidity sounder based on real-time thermal emission from lunar surface. *Science China Earth Sciences*, *64*(3), 494-502. doi: 10.1007/s11430-020-9701-1

Low, F. J., & Davidson, A. W. (1965, October). Lunar Observations at a Wavelength of 1 Millimeter. *Astrophysical Journal*, *142*, 1278. doi: 10.1086/148405

Pardo, J. R., Serabyn, E., & Wiedner, M. C. (2005, November). Broadband submillimeter measurements of the full Moon center brightness temperature and application to a lunar eclipse. *Icarus*, *178*(1), 19-26. doi: 10.1016/j.icarus.2005.04.005

Reber, E. E., & Stacey, J. M. (1969, March). 1. 4-mm and 3. 4-mm Observations of the Lunar Eclipse on 18 October 1967. *Icarus*, *10*(2), 171-178. doi: 10.1016/0019-1035(69)90019-0

Sandor, B. J., & Clancy, R. T. (1995, June). Microwave observations and modeling of a lunar eclipse. *Icarus*, *115*(2), 387-398. doi: 10.1006/icar.1995.1106

Sinton, W. M. (1956, March). Observation of a Lunar Eclipse at 1.5 MM. *Astrophysical Journal*, *123*, 325. doi: 10.1086/146165

Yang, H., & Burgdorf, M. (2020, April). A Study of Lunar Microwave Radiation Based on Satellite Observations. *Remote Sensing*, *12*(7), 1129. doi: 10.3390/rs12071129